

Promoting mechanism of potassium in preferential CO oxidation on Pt/Al₂O₃

Masatoshi Kuriyama ^a, Hisanori Tanaka ^a, Shin-ichi Ito ^a, Takeshi Kubota ^b,
Toshihiro Miyao ^c, Shuichi Naito ^c, Keiichi Tomishige ^{a,*}, Kimio Kunimori ^{a,*}

^a Institute of Materials Science, University of Tsukuba, 1-1-1 Tennodai,
Tsukuba, Ibaraki 305-8573, Japan

^b Department of Material Science, Shimane University, Matsue 690-8504, Japan

^c Department of Applied Chemistry, Faculty of Engineering, Kanagawa University,
3-27-1 Rokkakubashi, Kanagawa-ku, Yokohama, Kanagawa 221-8686, Japan

Corresponding authors

Kimio Kunimori

Tel: +81-29-853-5026, Fax: +81-29-853-4490, E-mail: kunimori@ims.tsukuba.ac.jp

Keiichi Tomishige

Tel and Fax: +81-29-853-5030, E-mail: tomi@tulip.sannet.ne.jp

Abstract

Addition of potassium enhanced the activity of preferential CO oxidation on Pt/Al₂O₃. The additive effect of potassium weakened the interaction between CO and Pt, and it also changed the CO adsorption site. FT-IR observation under the PROX condition suggests the presence of adsorbed species derived from O₂ and H₂ such as OH species, which can be related to the promoting effect of H₂ presence in the PROX reaction.

Keywords: preferential CO oxidation, platinum, Al₂O₃, potassium

1. Introduction

Hydrogen is a promising energy carrier associated with the fuel cell technology [1], where one of hydrogen production methods is the steam reforming reaction of hydrocarbons and oxygenates. In this case, the product of gases can contain CO as an impurity, and this can be regarded as a poison for the anode catalyst [2-4]. Preferential CO oxidation in H₂-rich mixtures is an important reaction in terms of the purification of the fuel gas [5].

There have been a lot of reports on supported noble metal catalysts such as Pt [6-33], Pd [15, 34], Ru [15,35] and Rh [36-39] for the preferential CO oxidation in H₂-rich gas. In particular, the effect of various additives has been investigated [6,11,18,19,24,25,27]. In addition, Au [40-46] and Cu [47-50] catalysts also exhibited high performance, and these behaviors can be generally explained by the weaker interaction with CO compared to noble metal catalysts. Recently, the addition of alkali metal to noble metal catalysts has been reported in the preferential CO oxidation [6-8,34, 36-39]. It has been reported that the Pt clusters supported on Cs-modified SiO₂ showed higher turnover rates selectivity than the clusters of similar size dispersed on SiO₂ and Al₂O₃, and the modification effect can be explained by the disruption of CO monolayer growth by promoting the formation of unreactive chemisorbed carbon via CO dissociations and disproportionation [6]. In contrast, in the case of Pt/Al₂O₃ modified with potassium, it has been reported that the adsorption site of CO on Pt was changed drastically and the interaction between CO and Pt becomes weaker with the addition of potassium [51]. Our group has reported that the optimized K-Pt/Al₂O₃ catalyst was very effective in decreasing CO concentration below 10 ppm in the fuel gas, and in particular the activity of CO oxidation was promoted drastically by the presence of H₂ [7,8]. In this article, we investigated the effect of potassium on catalytic properties in the preferential CO oxidation by

means of transmission electron microscopy (TEM), extended X-ray adsorption fine structure (EXAFS), X-ray near edge structure (XANES) and *in-situ* Fourier transform infrared spectroscopy (FT-IR). In particular, we attempted to elucidate the promoting mechanism of potassium on Pt/Al₂O₃ in the preferential CO oxidation was discussed.

2. Experimental

2.1. Catalyst preparation

The Al₂O₃ support (JRC-ALO-4 from Japan Reference Catalyst (JRC); BET surface area, 170 m²/g) was used as support materials. Before the impregnation, Al₂O₃ was calcined for 3 h in air at 873 K. Pt/Al₂O₃ catalyst was prepared by impregnating the Al₂O₃ with an aqueous solution of Pt(NO₂)₂(NH₃)₂ (Soekawa Chemical Co., Ltd.). After the impregnation, the sample was dried at 383 K for 12 h, and then calcined in air at 773, 823 and 873 K for 3 h. Calcination temperature of the catalysts is denoted in an angle bracket like Pt/Al₂O₃ [773]. The loading amount of Pt was 2 wt%. The Pt/Al₂O₃ catalysts modified with potassium were also prepared, and the modification method was as follows. After the impregnation with the aqueous solution of Pt(NO₂)₂(NH₃)₂, the sample was dried at 383 K for 12 h. After the further impregnation of the dried sample with an aqueous solution of KNO₃ (Wako Pure Chemical Industries, Ltd.), it was dried again at 383 K for 12 h, and calcined at 773 K for 3 h. The loading amount of potassium is described in the molar ratio to Pt (K/Pt=10). The Pt/Al₂O₃ catalysts modified with potassium are denoted as K-Pt/Al₂O₃ and the molar ratio of K/Pt is shown in a parenthesis like K-Pt/Al₂O₃ (10). The catalysts were reduced with hydrogen at 773 K for 1 h in the reactor before the activity test.

2.2. Activity test of preferential CO oxidation and related reactions

Preferential CO oxidation in H₂-rich gas was carried out in a fixed-bed flow reaction system at atmospheric pressure using 100 mg of the catalyst at the total flow rate of 100 cm³/min (STP) (GHSV= 30,000 h⁻¹). The feed stream contained 0.2% CO, 0.2% O₂ and 75% H₂, and it was balanced with helium. The effluent gas was analyzed using an on-line gas chromatograph (GC) system equipped with a TCD detector. The activity was evaluated by CO and O₂ conversions, which can be calculated on the basis of CO and O₂ concentrations in the reactant gas and the effluent gas. The selectivity of CO oxidation is defined as the ratio of O₂ consumption for the CO oxidation to the total O₂ consumption. The preferential CO oxidation in H₂-rich stream is denoted as PROX here. As a reference, we also carried out the activity test of CO oxidation in the absence of H₂. Here, the feed stream contained 0.2% CO, 0.2% O₂, and it was balanced with helium. This CO oxidation in the absence of H₂ is denoted as CO+O₂. As another reference, the activity of the water gas shift reaction was also tested, and the feed contained 0.2% CO, 3% H₂O balanced with He. The steam is introduced by a gas stripping method. In all reactions, the activity was observed during 30 min at each condition. Since almost no deactivation was observed, the results of the activity test correspond to those under the steady-state condition.

2.3. Catalyst characterization

2.3.1. Measurement of adsorption amount of CO and H₂

The catalysts were characterized by the amount of H₂ and CO adsorption. The amount of the irreversible adsorption of H₂ and CO (H/Pt, CO/Pt) was measured at room temperature in a vacuum system (sample weight: 0.15 g, dead volume: 65 cm³) by the volumetric method [38]. The samples are pretreated in O₂ at 773 K for 1 h, followed by H₂ reduction at 773 K for 1 h at atmospheric pressure. The equilibrium pressure of H₂ and CO was about 1.0 kPa.

2.3.2. TEM observation

Transmission electron microscope (TEM) images were taken by means of JEM-2010F (JEOL) equipment operated at 200 kV. First, the catalysts were reduced by H₂ pretreatment at 773 K for 1 h in a fixed-bed reactor. After the reduction, samples were stored under vacuum until the measurements. Samples were dispersed in 2-propanol using supersonic waves, and they were put on Cu grids for TEM observation under air atmosphere. Average particle size (d) is calculated by $d = \frac{\sum n_i d_i^3}{\sum n_i d_i^2}$ (n_i : number of pieces, d_i : particle size) [52].

2.3.3. EXAFS and XANES

Pt L_3 -edge EXAFS and XANES spectra was measured at the BL-12C station of the Photon Factory at the High Energy Accelerator Research Organization (Proposal No. 2005G041). The storage ring was operated at 2.5 GeV. A Si (111) single crystal was used to obtain a monochromatic X-ray beam. The monochromator was detuned to 60% maximum intensity to avoid higher harmonics in the X-ray beam. Two ion chambers filled with Ar and 15 % Ar diluted N₂ for Pt L_3 -edge EXAFS were used, respectively, as detectors of I and I_0 . The samples for the measurement were prepared by pressing 200 mg of catalyst powder to disks. The thickness of the samples was chosen to be 0.6-0.7 mm (10 mm ϕ) to give an edge jump of 0.7. The samples were pretreated at 773 K with H₂ for 1 h. After the pretreatment, we transferred the samples to the measurement cell without exposing the sample disk to air, using a glove box filled with nitrogen. EXAFS and XANES data were collected in a transmission mode at room temperature. For EXAFS analysis, the oscillation was first extracted from the EXAFS data by a spline smoothing method [53]. The oscillation was normalized by the edge height around 50 eV. The Fourier transformation of the k^3 -weighted EXAFS oscillation from k space to r space was performed over the range 30-160 nm⁻¹

to obtain a radial distribution function. The inversely Fourier filtered data were analyzed by a common curve-fitting method [54,55]. For the curve-fitting analysis, the empirical phase shift and amplitude functions for Pt-Pt, Pt-O bonds were extracted, respectively from the data for Pt foil and $\text{Na}_2\text{Pt}(\text{OH})_6$. In the analysis of XANES spectra, the normalized spectra were obtained by subtracting the pre-edge background from the raw data with a modified Victoreen's equation and normalizing them by the edge height [56-59]. Analysis of EXAFS data was performed using the "REX2000" program (Version: 2.3.3; Rigaku Corp.).

2.3.4. FT-IR measurement

Fourier transform infrared (FT-IR) spectra were recorded with a Nicolet Magna 550 spectrometer equipped with a MCT detector (resolution: 4 cm^{-1}) in a transmission mode, using an in-situ IR quartz cell with CaF_2 windows. All samples for the IR measurement were pressed into self-supporting wafers with a diameter of 20 mm and a weight of about 300 mg. The sample disk was transferred to the IR cell connected to the closed circulation systems, and the samples were reduced with H_2 at 773 K for 1 h at 13 kPa. After the pretreatment, the sample was cooled down to 313 K, and the gases (CO , $\text{CO}+\text{O}_2$, $\text{CO}+\text{O}_2+\text{H}_2$) were introduced to the IR cell connected to the flow and evacuating system. Temperature dependence of FT-IR spectra during the reactions was measured for 15 min at each temperature. FT-IR spectra of adsorbed species were obtained by subtracting the spectra before the reaction at the same temperature. The total gas flowing rate in all the reactions was adjusted to $\text{GHSV}=30,000\text{ h}^{-1}$, which was used for the activity tests in the fixed bed reactor.

3. Results and discussion

3.1. Catalytic performance in PROX and CO+O₂

Figure 1 shows the reaction temperature dependence of the performance of PROX and CO+O₂ reactions. K-Pt/Al₂O₃ (10) showed much higher activity and selectivity than all the Pt/Al₂O₃ catalysts in the PROX reaction [7,8]. The CO conversion in the PROX on K-Pt/Al₂O₃ (10) reached almost 100 % in the temperature range of 383 – 430 K. This behavior is useful because it avoids a careful temperature control. In particular, according our previous report, K-Pt/Al₂O₃ (10) gave CO concentration lower than 10 ppm as a result of the PROX reaction in the temperature range of 375-410 K [7]. As shown in Figure 1 (a), the CO conversion in the PROX reaction was much higher than that of CO+O₂ reaction, and this suggests that the presence of H₂ promotes the CO oxidation remarkably on K-Pt/Al₂O₃ (10). In contrast, as shown in Figure 1 (b), the CO conversion in the PROX reaction on Pt/Al₂O₃ [773] was lower than that in the CO+O₂ reaction at the reaction temperatures higher than 420 K. This can be related to the low selectivity of CO oxidation in PROX on Pt/Al₂O₃ [773]. The amounts of CO and H₂ adsorption on K-Pt/Al₂O₃ (10) and three Pt/Al₂O₃ catalysts are listed in Table 1. The adsorption amount of the Pt/Al₂O₃ catalysts decreased gradually with increasing calcination temperature due to aggregation of Pt metal particles. It should be noted that the CO adsorption amount of K-Pt/Al₂O₃ (10) was comparable to that of Pt/Al₂O₃ [823]. Based on the result of CO adsorption, it is possible to estimate the turnover frequency (TOF) of CO oxidation as also listed in Table 1. Regarding the Pt/Al₂O₃ catalysts, the TOF in PROX increases gently with decreasing adsorption amount and metal dispersion. This tendency agrees with the results of the previous report [33]. It has been reported that flat surfaces have a significantly higher CO oxidation activity per surface site compared with low-coordination edge and corner atoms in the

PROX reaction [33]. In addition, it is characteristic that K-Pt/Al₂O₃ (10) gave much higher TOF of CO oxidation in PROX than the Pt/Al₂O₃ catalysts. Furthermore, the TOF in PROX was much higher than that in CO+O₂ on K-Pt/Al₂O₃ (10). One of the promoting mechanisms of H₂ to CO oxidation may be due to the water gas shift reaction originated from H₂ oxidation to H₂O on the basis of the previous reports [9,23-27]. Therefore, the activity of the water gas shift reaction was also measured and the TOF obtained is listed in Table 1. As a result, the TOFs of water gas shift reaction were much lower than these in PROX and CO+O₂, and the promotion of H₂ to CO oxidation cannot be explained by the water gas shift reaction in the present case.

3.2. Catalyst characterization by means of TEM, EXAFS and XANES

Figure 2 shows the TEM images of Pt/Al₂O₃ [773] and K-Pt/Al₂O₃ (10) catalysts. Average of particle size of Pt/Al₂O₃ [773] and K-Pt/Al₂O₃ (10) were determined to be 0.5 ± 0.1 and 2.0 ± 0.3 nm, respectively. The tendency that K-Pt/Al₂O₃ (10) has lower dispersion than Pt/Al₂O₃ [773] agrees well with the results of adsorption amount (Table 1).

Figure 3 shows the result of Pt L₃-edge EXAFS analysis of these catalysts, and curve fitting results are listed in Table 2. In the case of curve fitting of Pt/Al₂O₃ [773] and [823], the Pt-Pt and Pt-O bonds were required, although the contribution of the Pt-O bond is rather small. This suggests that highly dispersed Pt metal particles have an interaction with the surface of Al₂O₃ support. The coordination number of the Pt-Pt bond on Pt/Al₂O₃ increased monotonously with increasing of the calcination temperature. It is concluded that aggregation of Pt metal particles occurs by calcination at higher temperature. The coordination number of the Pt-Pt bond on K-Pt/Al₂O₃ (10) was located between Pt/Al₂O₃ [773] and [823], and the tendency is similar to that of the adsorption amount of CO. This can be related to the neutralization of the acidic properties of Al₂O₃, which can contribute

to the enhancement of metal dispersion.

Figure 4 shows the results of Pt L₃-edge XANES spectra, and the results of the XANES analysis are listed in Table 3. It has been known that the white line intensity of Pt L₃-edge is an informative indication for the electronic state of Pt: larger white line is due to more electron vacancy in d-orbital [60]. As reported previously, a relative electron deficiency of the Pt species can be evaluated from white line intensity [56-59]. The relative electron deficiency decreases gradually with increasing the calcination temperature in the case of the Pt/Al₂O₃ catalysts. This can be associated with the decrease of the contribution of the Pt-O bond in EXAFS results and the decrease of metal dispersion. On the other hand, the relative electron deficiency of K-Pt/Al₂O₃ (10) is positioned between Pt/Al₂O₃ [773] and [823]. In order to discuss the electronic state of the catalysts considering the Pt metal particle size, the relation between the coordination number of the Pt-Pt bond obtained from EXAFS and the relative electron deficiency from XANES is shown in Figure 5. In the case of the Pt/Al₂O₃ catalysts, the relative electron deficiency decreased gradually with increasing the coordination number of the Pt-Pt bond. In contrast, K-Pt/Al₂O₃ (10) is far from the relation of the Pt/Al₂O₃ catalysts, and this means that Pt metal particles in K-Pt/Al₂O₃ (10) have higher electron deficiency for the large Pt-Pt coordination number, and this can be caused by the modification of potassium. As is usually known, the additive effect of alkali metal to metal surfaces is explained by the electron transfer from the alkali metal to the metal surface [61-63]. This tendency is opposite to the results above. The difference is due to the chemical state of alkali metal; here potassium is present as a cation, not metallic. The chemical state of the potassium was investigated by the temperature programmed reduction with H₂. In the profile, the peak of H₂ consumption peak due to the reduction of potassium ions to metal species was not observed.

Therefore, the potassium was not metallic even after the H₂ reduction.

3.3. Behavior of adsorbed CO during the reaction using *in-situ* FT-IR

Figure 6 shows the effect of evacuation temperature on IR spectra of CO adsorption over K-Pt/Al₂O₃ (10) and Pt/Al₂O₃ [773]. On K-Pt/Al₂O₃ (10), three peaks were observed. The peaks at 2059 and 1979 cm⁻¹ can be assigned to linear and bridge CO on Pt, respectively [51]. It should be noted that the peak at 1760 cm⁻¹ was observed, which was not observed on Pt/Al₂O₃, and it has been suggested that the peak can be assigned to a three-fold coordinated CO species on the Pt atoms interacting with potassium species [51]. Linear, bridge and three-fold CO are denoted as L-CO, B-CO and T-CO, respectively. The changes of the peak intensities are plotted in Figure 6 (III). Almost all the CO adsorbed on K-Pt/Al₂O₃ (10) was desorbed at 513 K, on the other hand, major CO on Pt/Al₂O₃ [773] remained even at the temperature of 633 K. This indicates that the interaction of CO with K-Pt/Al₂O₃ (10) is much weaker than that with Pt/Al₂O₃ [773]. This behavior agrees with the results of the previous report [51], and this can be also related to the higher relative electron deficiency of K-Pt/Al₂O₃ (10).

Figure 7 shows the temperature dependence of IR spectra of K-Pt/Al₂O₃ (10) during the PROX and CO+O₂ reactions and the CO introduction. The spectrum in the CO introduction at 313 K was almost the same as that in Figure 6 (I), however, the different point is that CO can be adsorbed even at 453 K in the presence of gas-phase CO (Figure 7 (c)). The peak intensities of L-CO, B-CO and T-CO are plotted in Figure 7 (f). The order of the peak intensity in this temperature range was as follows: T-CO > B-CO > L-CO. On the other hand, in the CO+O₂ reaction (Figure 7 (b)), the shape of the spectra is different from that in the CO introduction. As shown in Figure 7 (e), the order of the peak intensity in the range of 313-373 K was B-CO > L-CO ≈ T-CO, and the

intensity of T-CO decreased and that of B-CO increased significantly compared to the case of the CO introduction. Another important point is that all these three peaks during the CO+O₂ reaction were shifted to higher wavenumber (about 20-60 cm⁻¹) compared with those during the CO introduction. According to the previous report, adsorbed oxygen atom occupies the three-fold hollow site of Pt (111) surface [64]. In the case of the coadsorption of oxygen atom and CO, oxygen atom is adsorbed on the three-fold site and CO is adsorbed mainly on the on-top site over Pt (111), Pd (111) and Rh (111) [64,65]. The coadsorption affects the adsorption site of CO strongly, and this suggests that the adsorption site of CO can be shifted to the site with lower coordination number. This can explain the change of adsorption site during the CO+O₂ reaction. In addition, the peak position of adsorbed CO was shifted to higher wavenumber by the coordination of oxygen atom [65]. From the comparison between the CO+O₂ reaction and the CO introduction, the peak shift and the ratio change of the CO adsorption sites suggest that coadsorption of CO and oxygen occurs during the CO+O₂ reaction. In addition, the increase of the absorbance around 1700 cm⁻¹ can be due to adsorbed carbonate species originated from CO₂ produced by CO oxidation. Furthermore in the case of CO+O₂, the peaks disappeared suddenly above 393 K (Figure 7 (b)). This represents the increase of oxygen coverage and the decrease of CO coverage at higher reaction temperature, which is expected from the kinetics of CO oxidation with O₂ [66, 67]. Figures 7 (a) and (b) show the behavior during PROX. The spectrum of PROX at 313 K was similar to that of CO+O₂, and the order was B-CO > T-CO ≈ L-CO. However, the shift of B-CO and T-CO of PROX was smaller than that of CO+O₂. It should be noted that total peak area (L-CO+B-CO+T-CO, Figure 7 (d)) of PROX decreased gently with increasing reaction temperature, and the decrease of PROX in the temperature range of 313-373 K was more significant than that of CO+O₂. As shown in Figure 7 (c),

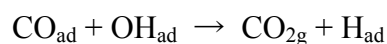
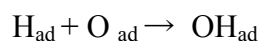
CO can be adsorbed on K-Pt/Al₂O₃ (10) when CO is present in the gas phase. Based on this result, the presence of another adsorbed species with considerable coverage is suggested during PROX. Considering that the peak shift of PROX is smaller than that of CO+O₂, the adsorbed species can have the lower ability to accept electrons from Pt than oxygen atom. It is expected that adsorbed species can be formed in the simultaneous presence of H₂ and O₂, and that candidates of the species are H₂O₂ and OOH. However, considering that Pt is usually unsuitable to the production of H₂O₂ from H₂ and O₂, these are unlikely. Another plausible candidate is hydroxide species (OH). The OH group may be observed in FT-IR spectra in higher wavenumber region, however, in fact, it is difficult because the peaks due to H₂O, which is a byproduct of the PROX, are overlapped, and therefore we don't have the direct evidence of the OH group on Pt at present. Discussion on the species and the reaction mechanism is also mentioned later.

Figure 8 shows temperature dependence of IR spectra of Pt/Al₂O₃ [773] during the PROX and CO+O₂ reactions and the CO introduction. Regarding Pt/Al₂O₃ [773], the spectra under these three conditions seem to be similar below 433 K. This means that the coverage of adsorbed CO is close to the saturation level, and the coverage of coadsorbed species is rather small. The difference of the peak position is so small and this supports the above interpretation. At temperature higher than 443 K in the CO+O₂ reaction, the peaks disappeared like the case of K-Pt/Al₂O₃ (10), although the temperature on Pt/Al₂O₃ [773] is much higher than that on K-Pt/Al₂O₃ (10). This can be explained by the stronger interaction of CO with Pt/Al₂O₃ [773] as shown in Figure 6.

3.4. Promoting effect of potassium on the preferential CO oxidation over Pt/Al₂O₃

Addition of potassium weakens the interaction between Pt and CO. This can be caused by the increase of electron deficiency of Pt species. This can contribute to high activity at lower reaction

temperature. Another important point is that the adsorption site of CO is changed drastically. On K-Pt/Al₂O₃ (10), bridge and three-fold hollow CO species were clearly observed. The reason of the adsorption site change is not elucidated at present, however, it can be related to the change in the electronic state of Pt modified by potassium. Based on the results of in-situ FT-IR observation, the coverage of CO on K-Pt/Al₂O₃ (10) during PROX was lower and the presence of another coadsorbed species than oxygen atom is suggested. This species can promote the CO oxidation, and one possible candidate is the OH group which can be formed by adsorbed hydrogen and oxygen atoms. It has been reported that the OH group promoted CO oxidation on Pt (111) [63,68], as described below.



These reaction formulas correspond to the reaction route via OH species as an autocatalytic mechanism [68]. In fact, the presence of H₂ enhances the CO oxidation activity on Pt/Al₂O₃ at the reaction temperatures lower than 420 K (Figure 1 (b)), however, the effect is not so significant as that on K-Pt/Al₂O₃ (10) (Figure 1 (a)). This difference in the promoting effect of H₂ can be due to the difference in the coverage of the OH species, and potassium plays very important role in the enhancement of the OH coverage, for example, by Coulomb interaction between OH⁻ and K⁺. In addition, judging from the low activity of the water gas shift reaction, this active OH cannot be formed from H₂O in the gas phase.

4. Conclusions

- 1) The addition of potassium to Pt/Al₂O₃ enhanced the activity of the preferential CO oxidation

in H₂-rich stream remarkably. In particular, the presence of H₂ promoted the CO oxidation drastically.

2) According to the catalyst characterization by means of TEM and EXAFS, K-Pt/Al₂O₃ (10) had metal particles with about 2 nm diameter. As a result of Pt L₃-edge white line analysis, Pt metal particles on K-Pt/Al₂O₃ was electron deficient compared to those on the Pt/Al₂O₃ with similar metal particle size.

3) The CO adsorption on K-Pt/Al₂O₃ was much weaker than that on Pt/Al₂O₃ from the result of CO-TPD by FT-IR observation. This can be related to the electron deficiency of K-Pt/Al₂O₃.

4) FT-IR spectra suggest that CO is adsorbed on the bridge and three-fold hollow sites as well as on the on-top site on K-Pt/Al₂O₃, and this behavior was different from that on the Pt/Al₂O₃.

5) In-situ FT-IR observation under the PROX condition on K-Pt/Al₂O₃ at the low temperature, where the PROX reaction proceeds, indicated that the amount of CO adsorption was smaller than those in the CO+O₂ reaction and the CO introduction. This suggests that the adsorbed species originated from H₂ and O₂, for example the OH species, are present on the surface and it can promote the CO oxidation.

References

- [1] R. Farrauto, S. Hwang, L. Shore, W. Ruettinger, J. Lampert, T. Giroux, Y. Liu, O. Ilinich, *Annu. Rev. Mater. Res.* 33 (2003) 1.
- [2] B. Rohland and V. Plzak, *J. Power Source*, 84 (1999) 183.
- [3] J. Divisek, H. -F. Oetjen, V. Peinecke, V. M. Schmidt, U. Stimming, *Electrochimica Acta* 43 (1998) 3811.
- [4] C. Song, *Catal. Today* 77 (2002) 17.
- [5] D. L. Trimm, *Appl. Catal. A* 296 (2005) 1.
- [6] C. Pedrero, T. Waku, E. Iglesia, *J. Catal.* 233 (2005) 242.
- [7] Y. Minemura, S. Ito, T. Miyao, S. Naito, K. Tomishige, K. Kunimori, *Chem. Commun.* (2005) 1429.
- [8] Y. Minemura, M. Kuriyama, S. Ito, K. Tomishige, K. Kunimori, *Catal. Commun.* 7 (2006) 623.
- [9] A. Manasilp, E. Gulari, *Appl. Catal. B* 37 (2002) 17.
- [10] H. Igarashi, H. Uchida, M. Suzuki, Y. Sasaki, M. Watanabe, *Appl. Catal. A* 159 (1997) 159.
- [11] I. H. Son, A. M. Lane, *Catal. Lett.* 76 (2001) 151.
- [12] X. Liu, O. Korotkikh, R. Farrauto, *Appl. Catal. A* 226 (2002) 293.
- [13] A. Sirijaruphan, J. G. Goodwin, Jr., R.W. Rice, *J. Catal.* 221 (2004) 288.
- [14] M. J. Kahlich, H. A. Gasteiger, R. J. Behm, *J. Catal.* 171 (1997) 93.
- [15] S. H. Oh, R. M. Sinkevitch, *J. Catal.* 142 (1993) 254.
- [16] O. Korotkikh, R. Farrauto, *Catal. Today* 62 (2000) 249.
- [17] A. Fukuoka, M. Ichikawa, *Top. Catal.* 40 (2006) 103.
- [18] M. Kotobuki, A. Watanabe, H. Uchida, H. Yamashita, M. Watanabe, *J. Catal.* 236 (2005) 262.

- [19] M. Kotobuki, A. Watanabe, H. Uchida, H. Yamashita, M. Watanabe, *Appl. Catal. A* 307 (2006) 275.
- [20] A. Sirijaruphan, J. G. Goodwin, Jr., R. W. Rice, *J. Catal.* 224 (2004) 304.
- [21] M. M. Schubert, M. J. Kahlich, G. Feldmeyer, M. Huttner, S. Hackenberg, H. A. Gasteiger, R. J. Behm, *Phys. Chem. Chem. Phys.* 3 (2001) 1123.
- [22] C. Kwak, T. J. Park, D. J. Suh, *Appl. Catal. A* 278 (2005) 186.
- [23] E. Simsek, S. Ozkara, A. E. Aksoylu, Z. I. Onsan, *Appl. Catal. A* 316 (2006) 169.
- [24] M. Shou, K. Tanaka, *Catal. Lett.* 111 (2006) 115.
- [25] S. H. Cho, J. S. Park, S. H. Choi, S. H. Kim, *J. Power Sources* 156 (2006) 260.
- [26] J. L. Ayastuy, M. P. Gonzalez-Marcos, A. Gil-Rodriguez, J. R. Gonzalez-Velasco, M. A. Gutierrez-Ortiz, *Catal. Today* 116 (2006) 391.
- [27] J. L. Ayastuy, M. P. Gonzalez-Marcos, J. R. Gonzalez-Velasco, M. A. Gutierrez-Ortiz, *Appl. Catal. B* 70 (2007) 532.
- [28] J. L. Ayastuy, A. Gil-Rodriguez, M. P. Gonzalez-Marcos, M. A. Gutierrez-Ortiz, *Int. J. Hydrogen Energy* 31 (2006) 2231.
- [29] G. Uysal, A. N. Akin, Z. I. Onsan, R. Yildirim, *Catal. Lett.* 108 (2006) 193.
- [30] I. H. Son, *J. Power Sources* 159 (2006) 1266.
- [31] S. Monyanon, S. Pongstabodee, A. Luengnaruemitchai, *J. Power Sources* 163 (2006) 547.
- [32] E. Y. Ko, E. D. Park, K. W. Seo, H. C. Lee, D. Lee, S. Kim, *Catal. Today* 116 (2006) 377.
- [33] B. Atalik, D. Uner, *J. Catal.* 241 (2006) 268.
- [34] N. Iwasa, S. Arai, M. Arai, *Catal. Commun.* 7 (2006) 839.
- [35] Y. F. Han, M. J. Kahlich, M. Kinne, R. J. Behm, *Phys. Chem. Chem. Phys.* 4 (2002) 389.

- [36] H. Tanaka, S. Ito, S. Kameoka, K. Tomishige, K. Kunimori, *Catal. Commun.* 4 (2003) 1.
- [37] H. Tanaka, S. Ito, S. Kameoka, K. Tomishige, K. Kunimori, *Appl. Catal. A* 250 (2003) 255.
- [38] S. Ito, H. Tanaka, Y. Minemura, S. Kameoka, K. Tomishige, K. Kunimori, *Appl. Catal. A* 273 (2004) 295.
- [39] S. Ito, T. Fujimori, K. Nagashima, K. Yuzaki, K. Kunimori, *Catal. Today* 57 (2000) 247.
- [40] M. M. Schubert, V. Plzak, J. Garche, R. J. Behm, *Catal. Today* 76 (2001) 143.
- [41] B. Schumacher, Y. Denkwitz, V. Plzak, M. Kinne, R. J. Behm, *J. Catal.* 224 (2004) 449.
- [42] R. M. Torres Sanchez, A. Ueda, K. Tanaka, M. Haruta, *J. Catal.* 168 (1997) 125.
- [43] F. Arena, Pio Famulari, G. Trunfio, G. Borura, F. Frusteri, L. Spadaro, *Appl. Catal. B* 66 (2006) 81.
- [44] M. Shou, H. Takekawa, D. Y. Ju, T. Hagiwara, D. L. Lu, K. Tanaka, *Catal. Lett.* 108 (2006) 119.
- [45] M. Azar, V. Caps, F. Morfin, J. Rousset, A. Piednoir, J. Bertolini, L. Piccolo, *J. Catal.* 239 (2006) 307.
- [46] C. Rossignol, S. Arrii, F. Morfin, L. Piccolo, V. Caps, J. Rousset, *J. Catal.* 239 (2006) 307.
- [47] Y. Tanaka, T. Utaka, R. Kikuchi, K. Sasaki, K. Eguchi, *Appl. Catal. A* 238 (2003) 11.
- [48] J. Papavasiliou, G. Avgouropoulos, T. Ioannides, *Appl. Catal. B* 66 (2006) 167.
- [49] Y. Liu, Q. Fu, M.F. Stephanopoulos, *Catal. Today* 93-95 (2004) 241.
- [50] J. W. Park, J. H. Jeong, W. L. Yoon, C. S. Kim, D. K. Lee, Y. K. Park, Y. W. Rhee, *Int J Hydrogen Energy* 30 (2005) 209.
- [51] S. Derrouiche, P. Gravejat, B. Bassou, D. Bianchi, *Appl. Surf. Sci.* 253 (2007) 5894.
- [52] Y. Chen, K. Tomishige, K. Yokoyama and K. Fujimoto, *Appl. Catal. A: Gen.* 165 (1997) 335.

- [53] J. W. Cook and D. E. Sayers, *J. Appl. Phys.* 52 (1981) 5024.
- [54] K. Okumura, J. Amano, N. Yasunobu and M. Niwa, *J. Phys. Chem. B* 104 (2000) 1050.
- [55] K. Okumura, S. Matsumoto, N. Nishiaki and M. Niwa, *Appl. Catal. B* 40 (2003) 151.
- [56] T. Kubota, K. Asakura, N. Ichikuni, Y. Iwasawa, *Chem. Phys. Lett.*, 256 (1996) 445.
- [57] T. Kubota, K. Asakura, Y. Iwasawa, *Catal. Lett.*, 46 (1997) 141.
- [58] A. N. Mansour, J. W. Cook, Jr. and D. E. Sayers, *J. Phys. Chem.* 88 (1984) 2330.
- [59] J. A. Horsely, *J. Chem. Phys.*, 76 (1982) 1451.
- [60] H. Yoshida, Y. Yazawa, T. Hattori, *Catal. Today*, 87 (2003) 19.
- [61] Leonarda F. Liotta, Gut A. Martin, Giulio Deganello, *J. Catal.* 164 (1996) 322.
- [62] N. Pavlenko, P. P. Kostrobij, Y. Suchorski, R. Imbihl, *Surf. Sci.* 489 (2001) 29.
- [63] I. N. Yakovkin, V. I. Chernyi, A. G. Naumovets, *Surf. Sci.* 442 (1999) 81.
- [64] K. L. Kostov, P. Jakob, D. Menzel, *Surf. Sci.* 377 (1997) 802.
- [65] J. Libuda, H. -J. Freund, *Surf. Sci. Rep.*, 57 (2005) 157.
- [66] K. Nakao, S. Ito, K. Tomishige, K. Kunimori, *J. Phys. Chem. B* 109 (2005) 24002.
- [67] T. Engel, G. Ertl, *Adv. Catal.* 28 (1979) 1.
- [68] J. Bergeld, B. Kasemo, D. V. Chakarov, *Surf. Sci.* 495 (2001) L815.

Table 1 Adsorption amount of H₂, CO and TOF of CO₂ formation over K-Pt/Al₂O₃ and Pt/Al₂O₃ catalysts at 363 K.

Catalysts	Calcination temperature / K	Adsorption amount		TOF / $\times 10^{-3} \text{s}^{-1}$ ^{b)}		
		H/Pt ^{a)}	CO/Pt ^{a)}	CO+O ₂ ^{c)}	CO+O ₂ +H ₂ ^{d)}	CO+H ₂ O ^{e)}
K-Pt/Al ₂ O ₃ (10)	773	0.38	0.40	5.4	32 ^{f)}	1.3
Pt/Al ₂ O ₃ [773]	773	0.70	0.52	1.0	1.9	0.03
Pt/Al ₂ O ₃ [823]	823	0.53	0.37	-	2.2	-
Pt/Al ₂ O ₃ [873]	873	0.14	0.14	-	2.6	-

a) Irreversible adsorption of H₂ and CO at room temperature,

b) TOF of CO oxidation is calculated on the basis of CO/Pt,

c) 0.2% CO, 0.2% O₂, He balance,

d) 0.2% CO, 0.2% O₂, 75% H₂, He balance,

e) 0.2% CO, 3% H₂O, He balance.

f) The TOF was calculated by an extrapolating method in the Arrhenius plot at the temperature range of 323 – 353 K because K-Pt/Al₂O₃ (10) gave 88 % CO conversion at 363 K.

Table 2 Curve fitting results of Pt- L_3 edge EXAFS of K-Pt/Al₂O₃ (10) and Pt/Al₂O₃ catalysts after H₂ reduction.

Catalysts	Shells	C.N. ^a	$R / 10^{-1} \text{ nm}^b$	$\sigma / 10^{-1} \text{ nm}^c$	$\Delta E_0 / \text{eV}^d$	$R_f / \%^e$
Pt/Al ₂ O ₃ [773]	Pt-Pt	5.9±0.7	2.65±0.007	0.094±0.007	-4.7±1.8	0.94
	Pt-O	0.9±0.2	2.03±0.026	0.065±0.044	-5.7±7.1	
Pt/Al ₂ O ₃ [823]	Pt-Pt	7.6±0.6	2.78±0.002	0.093±0.002	6.5±0.5	1.0
	Pt-O	0.6±0.5	2.12±0.030	0.092±0.066	2.0±6.9	
Pt/Al ₂ O ₃ [873]	Pt-Pt	9.5±0.4	2.78±0.002	0.082±0.001	1.6±0.6	0.66
K-Pt/Al ₂ O ₃ (10)	Pt-Pt	8.5±0.3	2.74±0.003	0.080±0.012	-0.2±0.8	0.69

Sample pretreatment: reduction (H₂, 773 K, 1 h).

^a Coordination number, ^b Bond distance. ^c Debye-Waller factor,

^d Diffence in the origin of photoelectron energy between the reference and the sample,

^e Residual factor, Fourier filtering range: 0.16-0.38 nm.

Table 3 Results of Pt L_3 -edge XANES analysis of K-Pt/Al₂O₃ (10) and Pt/Al₂O₃ catalysts.

Catalysts	ΔA ^{a)}	A ^{b)}	$\Delta A / A$ ^{c)}
K-Pt/Al ₂ O ₃ (10)	0.78	-	0.102
Pt/Al ₂ O ₃ [773 K]	0.83	-	0.108
Pt/Al ₂ O ₃ [823 K]	0.66	-	0.085
Pt/Al ₂ O ₃ [873 K]	0.58	-	0.074
Pt foil	0.0	7.70	0

a) Area difference between catalysts and Pt-foil (11540-11566 eV),

b) White line area of Pt foil,

c) Relative electron deficiency.

Fig. 1 Reaction temperature dependence of CO conversion (■, △) and selectivity of CO oxidation (◆) in PROX and CO+O₂ reactions.

a: K-Pt/Al₂O₃ (10), b: Pt/Al₂O₃ [773], c: Pt/Al₂O₃ [823], d: Pt/Al₂O₃ [873]

Reaction conditions: PROX: 0.2% CO, 0.2% O₂, 75% H₂, He balance (■, ◆),

CO+O₂: 0.2% CO, 0.2% O₂, He balance (△).

Fig. 2 TEM images of (a) fresh Pt/Al₂O₃ [773] and (b) K-Pt/Al₂O₃ (10) after H₂ reduction.

Fig. 3 Results of Pt L₃-edge EXAFS analysis of K-Pt/Al₂O₃ (10) and Pt/Al₂O₃ catalysts after the H₂ reduction.

(I) k^3 -weighted EXAFS oscillations.

(II) Fourier transforms of k^3 -weighted Pt L₃-edge EXAFS, FT range: 30-160 nm⁻¹.

(III) Fourier filtered EXAFS data (solid line) and calculated data (broken line).

Fourier filtering range: 0.16-0.31 nm.

a: K-Pt/Al₂O₃ (10), b: Pt/Al₂O₃ [773], c: Pt/Al₂O₃ [823], d: Pt/Al₂O₃ [873].

Fig. 4 Pt L₃-edge XANES spectra of K-Pt/Al₂O₃ (10) and Pt/Al₂O₃ catalysts.

a: K-Pt/Al₂O₃ (10), b: Pt/Al₂O₃ [773], c: Pt/Al₂O₃ [823], d: Pt/Al₂O₃ [873]

Fig. 5 Relation between the relative electron deficiency from XANES and the coordination number of the Pt-Pt bond from EXAFS of K-Pt/Al₂O₃ (10) and Pt/Al₂O₃ catalysts.

Fig. 6 Effect of evacuation temperature on IR spectra of adsorbed CO on

(I) K-Pt/Al₂O₃ (10) and (II) Pt/Al₂O₃ [773] catalysts, and (III) Temperature dependence of total area of the CO adsorption peaks on the catalysts.

The samples were exposed to 0.3 kPa CO at 313 K and evacuated.

Fig. 7 Effect of temperature on IR spectra of K-Pt/Al₂O₃ (10) catalyst during PROX (a), CO+O₂ (b) reactions and CO (c) introduction, (d), (e), (f) Area of each peak as a function of temperature.

Reaction conditions: PROX: 0.2% CO, 0.2% O₂, 75 % H₂, He balance,

CO+O₂: 0.2% CO, 0.2%O₂, He balance,

CO: 0.2% CO, He balance

Fig. 8 Effect of temperature on IR spectra of Pt/Al₂O₃ catalyst during PROX (a), CO+O₂ (b) reactions and CO (c) introduction, (d) Area of the linear CO peak as a function of temperature.

□: L-CO(PROX), △: L-CO(CO+O₂), ◇L-CO(CO)

Reaction conditions: PROX: 0.2% CO, 0.2% O₂, 75 % H₂, He balance,

CO+O₂: 0.2% CO, 0.2%O₂, He balance,

CO: CO 0.2%, He balance

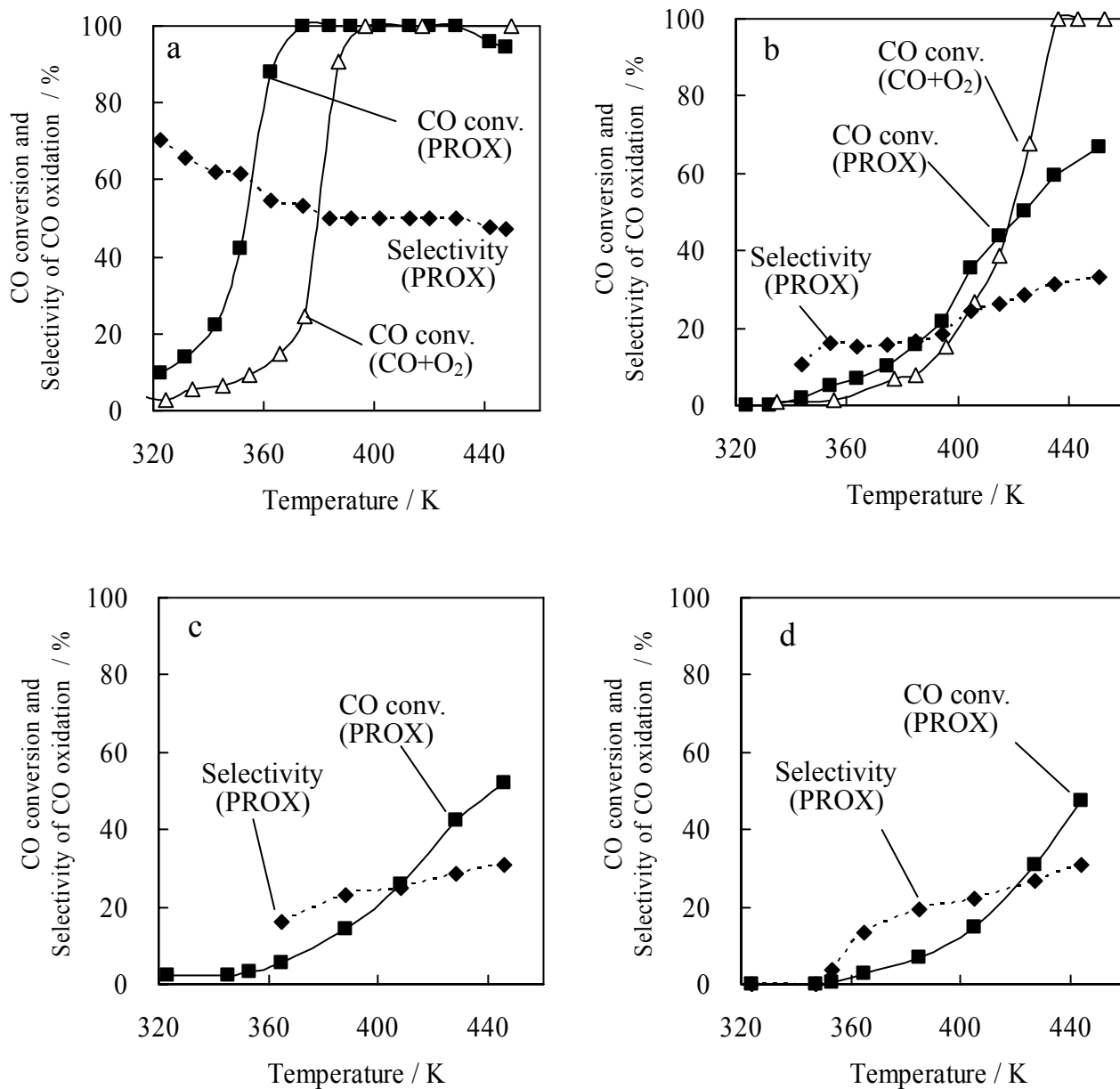


Fig. 1 Reaction temperature dependence of CO conversion (■, △) and selectivity of CO oxidation (◆) in PROX and CO+O₂ reactions.

a: K-Pt/Al₂O₃ (10), b: Pt/Al₂O₃ [773],

c: Pt/Al₂O₃ [823], d: Pt/Al₂O₃ [873]

Reaction conditions: PROX: 0.2% CO, 0.2% O₂, 75% H₂, He balance (■, ◆),

CO+O₂: 0.2% CO, 0.2% O₂, He balance (△).

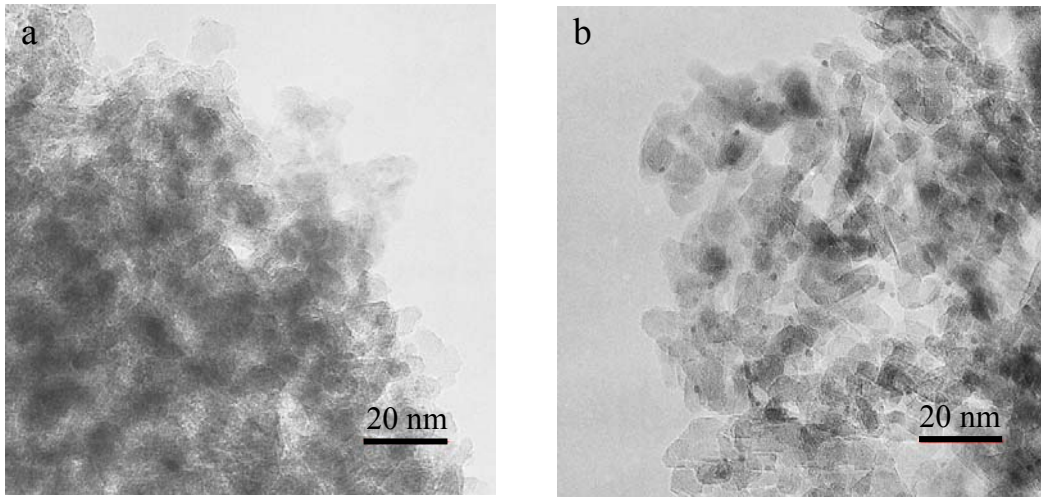


Fig. 2 TEM images of (a) fresh Pt/Al₂O₃ [773] and (b) K-Pt/Al₂O₃ (10) after H₂ reduction.

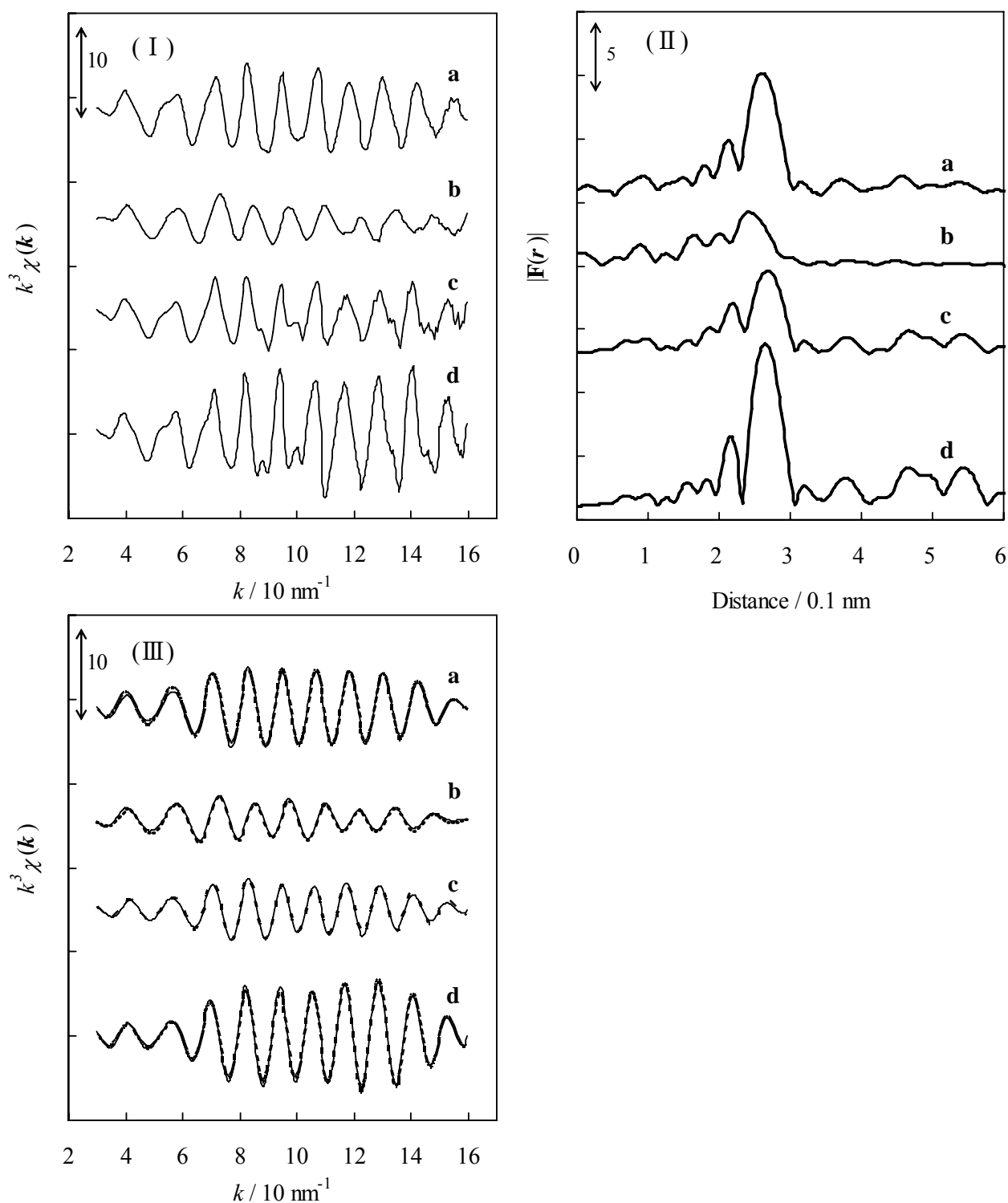


Fig. 3 Results of Pt L_3 -edge EXAFS analysis of K-Pt/ Al_2O_3 (10) and Pt/ Al_2O_3 catalysts after the H_2 reduction.

(I) k^3 -weighted EXAFS oscillations.

(II) Fourier transforms of k^3 -weighted Pt L_3 -edge EXAFS, FT range: 30-160 nm^{-1} .

(III) Fourier filtered EXAFS data (solid line) and calculated data (broken line).

Fourier filtering range: 0.16-0.31 nm.

a: K-Pt/ Al_2O_3 (10), b: Pt/ Al_2O_3 [773], c: Pt/ Al_2O_3 [823], d: Pt/ Al_2O_3 [873].

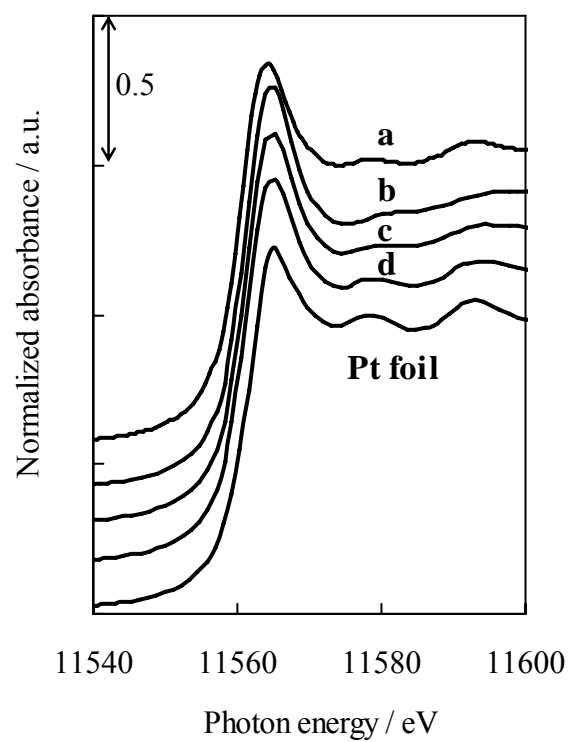


Fig. 4 Pt L₃-edge XANES spectra of K-Pt/Al₂O₃ (10) and Pt/Al₂O₃ catalysts.
a: K-Pt/Al₂O₃ (10), b: Pt/Al₂O₃ [773],
c: Pt/Al₂O₃ [823], d: Pt/ Al₂O₃ [873]

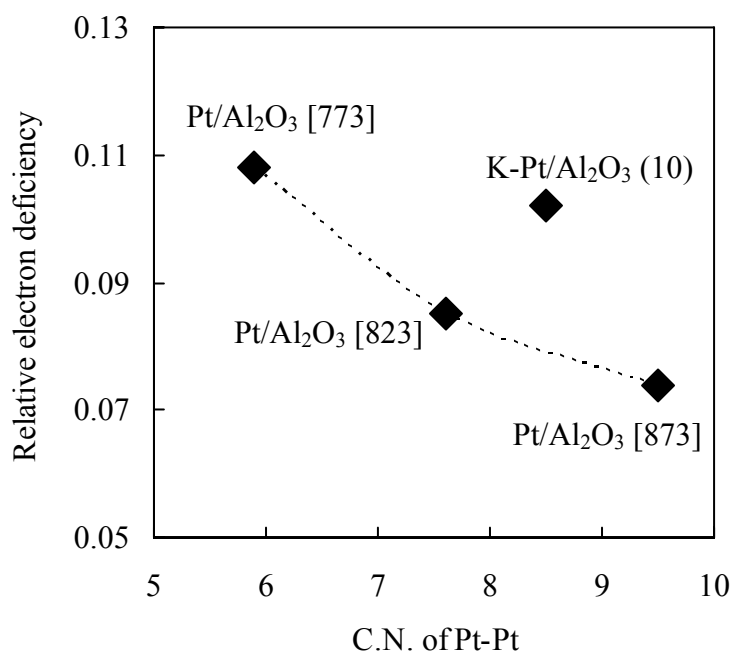


Fig. 5 Relation between the relative electron deficiency from XANES and the coordination number of the Pt-Pt bond from EXAFS of K-Pt/Al₂O₃ (10) and Pt/Al₂O₃ catalysts.

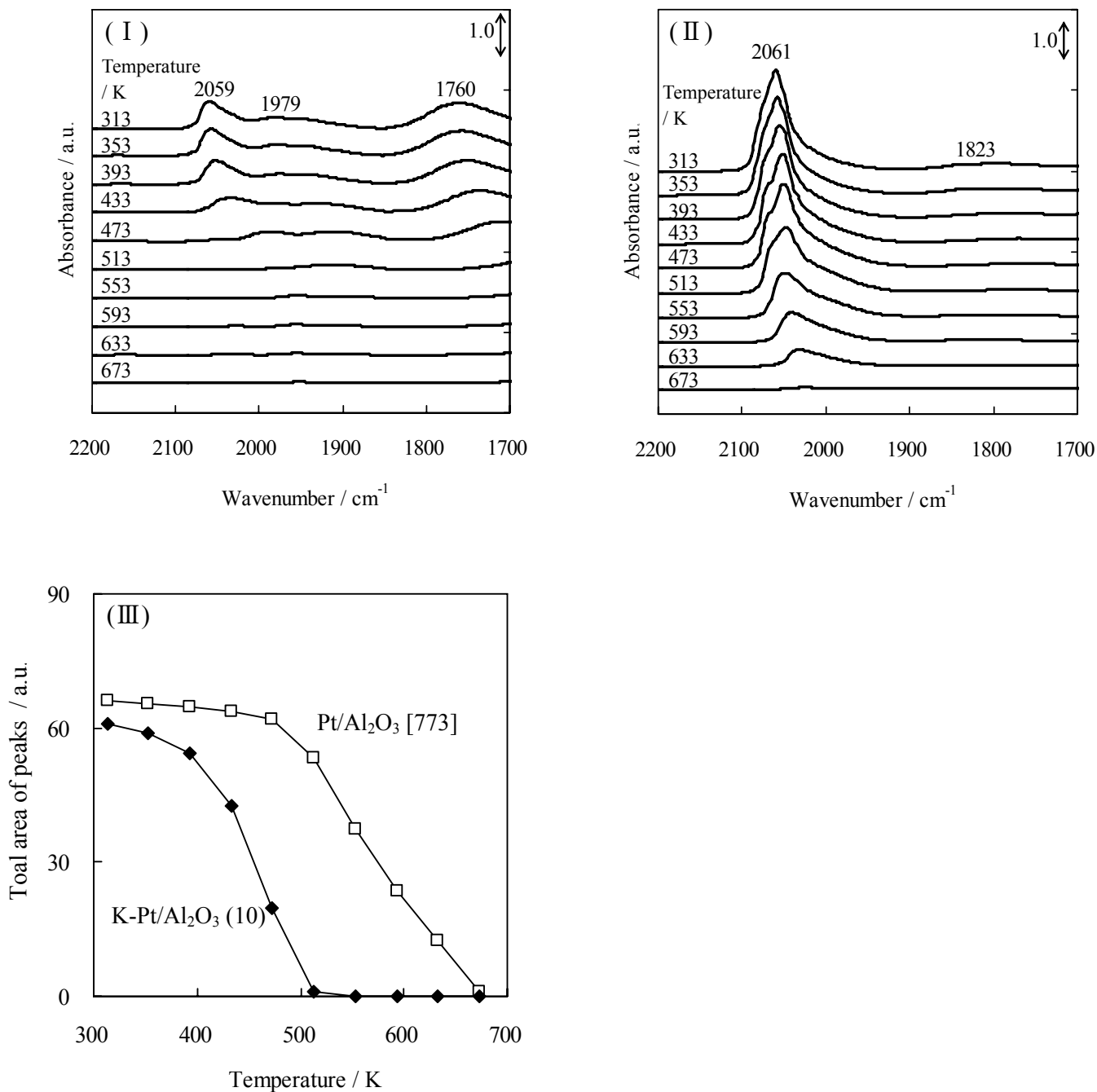


Fig. 6 Effect of evacuation temperature on IR spectra of adsorbed CO on (I) K-Pt/Al₂O₃ (10) and (II) Pt/Al₂O₃ [773] catalysts, and (III) Temperature dependence of total area of the CO adsorption peaks on the catalysts. The samples were exposed to 0.3 kPa CO at 313 K and evacuated.

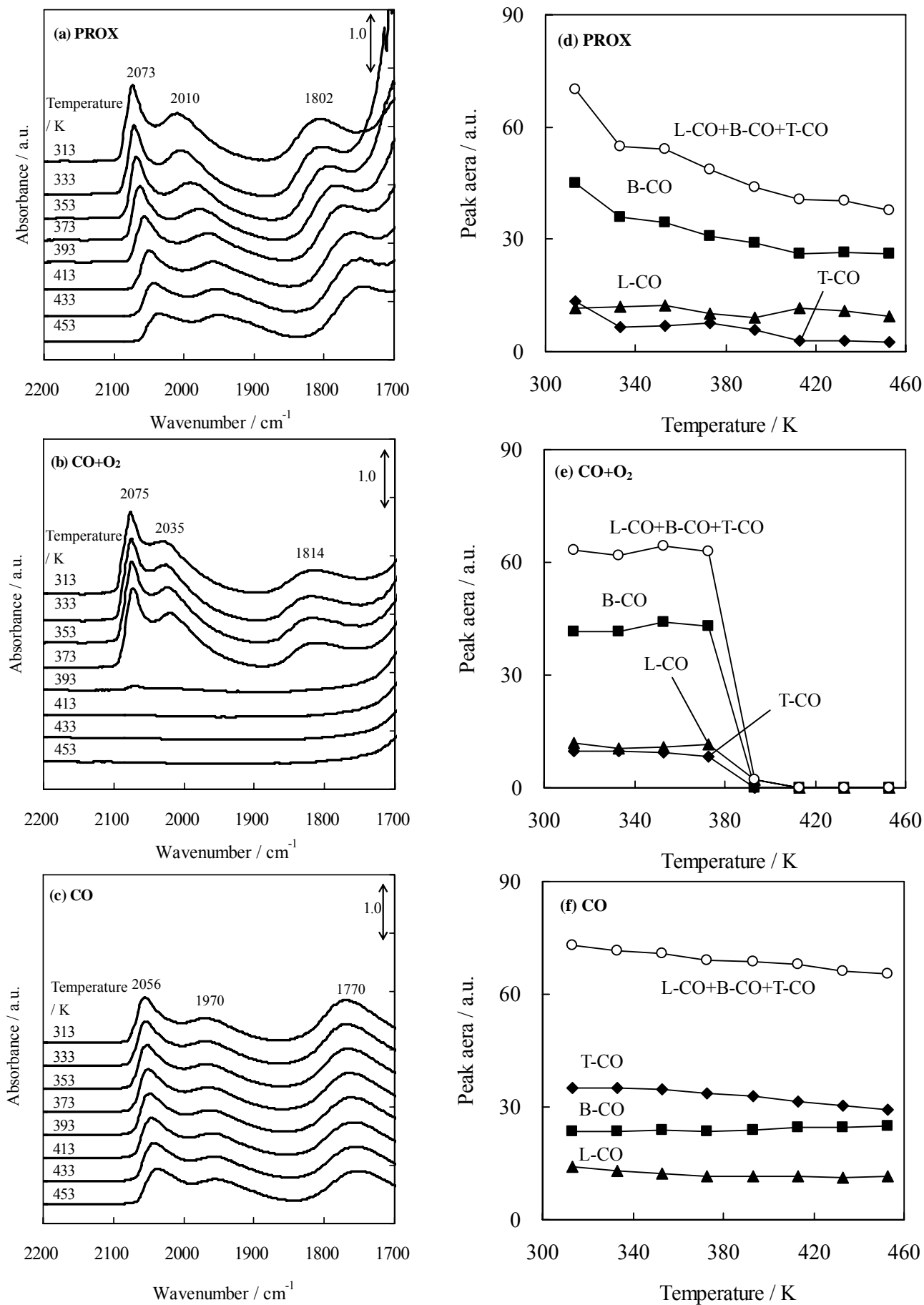


Fig. 7 Effect of temperature on IR spectra of K-Pt/Al₂O₃ (10) catalyst during PROX (a), CO+O₂ (b) reactions and CO (c) introduction, (d), (e), (f) Area of each peak as a function of temperature.

Reaction conditions: PROX: 0.2% CO, 0.2% O₂, 75 % H₂, He balance,
 CO+O₂: 0.2% CO, 0.2%O₂, He balance,
 CO: 0.2% CO, He balance

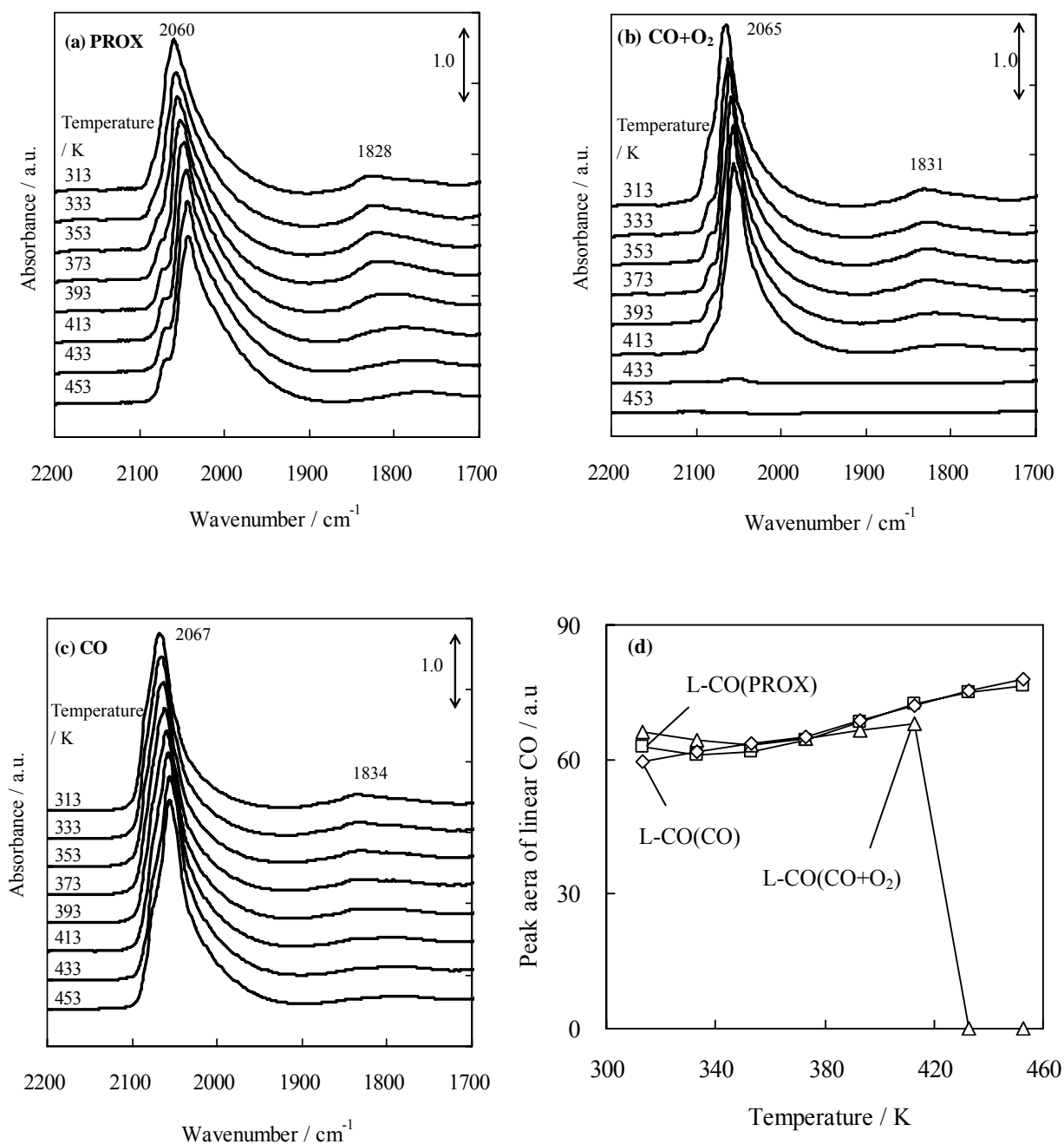


Fig. 8 Effect of temperature on IR spectra of Pt/Al₂O₃ [773] catalyst during PROX (a), CO+O₂ (b) reactions and CO (c) introduction, (d) Area of the linear CO peak as a function of temperature. □: L-CO(PROX), △: L-CO(CO+O₂), ◇L-CO(CO)
 Reaction conditions: PROX: 0.2% CO, 0.2% O₂, 75 % H₂, He balance,
 CO+O₂: 0.2% CO, 0.2%O₂, He balance,
 CO: CO 0.2%, He balance